Proton Conductive Polyimide Ionomer Membranes: Effect of NH, OH, and COOH Groups

JUMPEI SAITO,[1] MANABU TANAKA,[2] KENJI MIYATAKE,[2,3] MASAHIRO WATANABE[2]

[1]Interdisciplinary Graduate School of Medicine and Engineering, University of Yamanashi, 4 Takeda, Kofu 400-8510, Japan

[2]Fuel Cell Nanomaterials Center, University of Yamanashi, 6 Miyamae, Kofu 400-0021, Japan

[3]Division of Fuel Cell Research, Clean Energy Research Center, University of Yamanashi, 4 Takeda, Kofu 400-8510, Japan

Received 1 March 2010; accepted 4 April 2010
DOI: 10.1002/pola.24061
Published online in Wiley InterScience (www.interscience.wiley.com).

ABSTRACT: A new series of sulfonated polyimide (SPI) copolymers containing NH, OH, or COOH groups were synthesized by the polycondensation of 1,4,5,8-naphthalnetetracarboxylic dianhydride, 3,3′-bis(sulfopropoxy)-4,4′-diaminobiphenyl, and 3-(4-aminophenyl)-5-(3-aminophenyl)-1H-1,2,4-triazole (SPI-8-*m*), 3,5-bis(4-aminophenyl)-1H-1,2,4-triazole (SPI-8-*p*), 3,6-diaminocarbazole (SPI-9), 3,5-diamino-1H-1,2,4-triazole (SPI-10), bis(3-aminopropyl)-amine (SPI-11), 2,6-diaminopurine (SPI-12), 2,4-diamino-6-hydroxyprymidine (SPI-13), or 3,5-bis(4-aminophenoxy)benzoic acid (SPI-14). The obtained SPIs were soluble in polar organic solvents and gave tough and flexible membranes by solution casting. The SPI membranes having NH and COOH groups showed high thermal (decomposition temperature ≈200 °C) and mechanical (maximum stress >22 MPa) stability. Introducing NH groups, especially triazole and carbazole groups, was effective in improving proton conductive properties of SPI membranes at low humidity. © 2010 Wiley Periodicals, Inc. J Polym Sci Part A: Polym Chem 48: 2846–2854, 2010

KEYWORDS: fuel cells; ionomers; polyelectrolytes; polyimides; proton conduction

INTRODUCTION Polymer electrolyte membrane fuel cells (PEMFCs) have attracted considerable attention as an alternative energy source because of its high-energy efficiency and no emissions of pollutants. PEMFCs are expected for the applications to electric vehicles and stationary power sources.[1] However, improvement of performance and durability, and reduction of cost are needed before the practical applications.

Proton-conducting polymer electrolyte membranes are one of the key components in PEMFCs.[2–4] Polymer electrolyte membranes have to have high proton conductivity, high chemical and physical stability, and low gas permeability. Perfluorinated sulfonic acid (PFSA) ionomers such as Nafion NRE212 (Du Pont) have been most used. Although PFSA membranes are superior in terms of proton conductivity and durability, environmental inadaptability and production cost are issues. Therefore, there has been a great demand for nonfluorinated alternative PEMs.[5]

Sulfonated polyimides (SPIs) are one of the promising candidates as well as sulfonated polyethers.[6–13] They are readily available via typical polycondensation reaction of presulfonated diamine monomers and aromatic tetracarboxylic dianhydrides. Ion exchange capacity (IEC) of the SPIs can be easily controlled by copolymerizing with nonsulfonated diamine comonomers. High thermal stability and low gas permeability are attracting properties, whereas low proton conductivity under low humidity conditions and hydrolytic instability are major drawbacks of the SPI membranes. Okamoto and coworkers revealed that SPIs bearing pendant sulfonic acid groups are somewhat more proton conductive and more stable to hydrolysis.[14] However, SPIs require further improvement in the conductivity and stability.[15] The relationship between chemical structure and properties should be investigated in more detail.

We have previously reported synthesis and properties of sulfonated polyimides (SPI-8) containing 1,2,4-triazole groups in the main chains.[16] The introduction of triazole groups contributed to the improvement of thermal stability and mechanical properties. In addition, the SPI ionomers containing triazole groups showed higher proton conductivity than that of nontriazole-containing SPIs due to the increased water uptake. The membrane was durable for 5000 h in single fuel cell operation at 80 °C.[17,18] The objective of this research is to investigate the effect of NH, OH, and COOH groups on the properties of SPI membranes. A series of new SPI membranes containing triazole, carbazole, aliphatic amine, hydroxyl, and carboxylic acid groups have been synthesized. Their proton conductivity and gas permeability as well as

Additional Supporting Information may be found in the online version of this article. Correspondence to: K. Miyatake (E-mail: miyatake@yamanashi.ac.jp) or M. Watanabe (E-mail: m-watanabe@yamanashi.ac.jp)

Journal of Polymer Science: Part A: Polymer Chemistry, Vol. 48, 2846–2854 (2010)

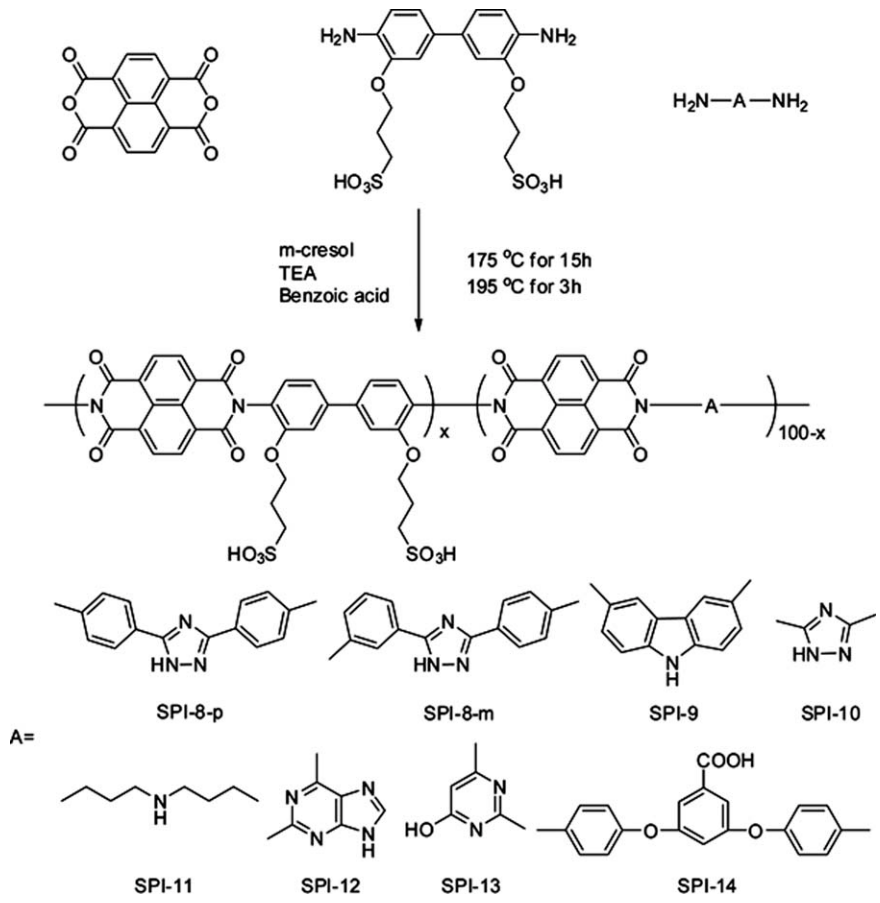

SCHEME 1 Synthesis of SPIs 8–14.

thermal, mechanical, and chemical stability have been measured and compared to one another.

RESULTS AND DISCUSSION

Synthesis and Characterization of SPI Copolymers

Synthetic procedure of the SPIs investigated in this study is shown in Scheme 1. *p*-APTAZ and *m*-APTAZ were synthesized by the condensation reaction of 4-aminobenzohydrazide with 4- or 3-aminobenzonitrile, respectively, under basic conditions. The purity of each APTAZ was confirmed by ^{1}H NMR and LC/MS analyses to be high enough for the polymerization reactions. Other nonsulfonated diamine monomers for SPI-9 to SPI-14 were commercially available. The polycondensation reaction of TCND, BSPA, and the nonsulfonated diamine comonomers was carried out in *m*-cresol in the presence of excess triethylamine (TEA). Molar percentage of BSPA to the nonsulfonated comonomers (X) was set as X = 50 (SPI-8-*p*, 8-*m*, and -9), 46 (SPI-11 and -12), 45 (SPI-13), and 56 (SPI-14) in order that the obtained copolymers have similar IEC values (~1.7 mequiv g^{-1}). As SPI-10 was only slightly soluble in *m*-cresol, DMSO, and NMP, when X = 43 (IEC = 1.77 mequiv g^{-1}), higher composition of BSPA (X = 50) and therefore higher IEC (1.95 mequiv g^{-1}) were adopted for SPI-10 with better solubility. All SPI copolymers, except for SPI-11, were obtained as fibers. GPC analyses revealed that SPI-8-*m*, -8-*p*, -9, and -10 copolymers were high molecular weight (M_w > 88.1 kDa, M_n > 44.9 kDa; Table 1). Other SPI copolymers (SPI-11, -12, -13, and -14) were relatively low molecular weight. The molecular weight of SPI-14 increased significantly from 9.6 kDa to 56.0 kDa in M_n or from 24.9 kDa to 174.8 kDa in M_w by drying under vacuum at 150 °C (SPI-14H), indicating possible crosslinking reaction via dehydration among carboxylic acid and/or sulfonic acid groups. ^{1}H NMR and IR spectra were compared between pristine SPI-14 and thermally treated SPI-14H. The intensity of symmetric C=O stretching vibration ascribed to carboxylic acid groups (1715 cm^{-1}) in the IR spectrum decreased slightly after the thermal treatment, whereas no changes were observed in the ^{1}H NMR spectra between SPI-14 and SPI-14H (see Supporting Information Figs. S1 and S2).

The SPI copolymers were characterized by ^{1}H NMR spectra. The ^{1}H NMR spectra are summarized in Figure 1, except for SPI-11, of which NMR analysis was not available due to its insufficient solubility in DMSO-d_6 and the other deuterated solvents. For the other SPIs, peaks were well-assigned to the supposed chemical structures. The peaks at 7.5–8.8 ppm were aromatic protons of the polyimides and the peaks at 1.8–4.3 ppm were aliphatic protons of the pendant groups. The two strong and sharp peaks designated with asterisk were due to ethanol used for washing the membranes. There were no evidences of side reactions (such as the reaction with NH, OH, and COOH groups) and/or residual amic acid groups. Copolymer composition and IEC value were

TABLE 1 Molar Percentage, Molecular Weight, IEC, and Density of SPI Membranes

Polymer	X^a	M_n (kDa)	M_w (kDa)	M_w/M_n	IEC[b] (mequiv g^{-1})	IEC[c] (mequiv g^{-1})	IEC[d] (mequiv g^{-1})	Density (g cm^{-3})	Membrane
SPI-8-*p*	50	56.6	191.8	3.4	1.70	1.68	1.76	1.49	Turbid, flexible
SPI-8-*m*	50	120.2	323.8	2.7	1.70	1.64	1.81	1.75	Turbid, flexible
SPI-9	50	56.1	109.3	1.9	1.78	1.58	1.76	1.60	Transparent, flexible
SPI-10	50	44.9	88.1	2.0	1.95	1.83	2.12	1.47	Turbid, flexible
SPI-11	46	13.1	23.6	1.8	1.76	–[f]	–[f]	–[f]	Turbid, brittle
SPI-12	46	4.8	10.7	2.2	1.76	–[f]	1.72	–[f]	Transparent, brittle
SPI-13	45	5.6	15.0	2.7	1.76	–[f]	1.77	–[f]	Transparent, brittle
SPI-14	56	9.6	24.9	2.6	1.76	1.51	1.64	–[f]	Transparent, rigid
SPI-14H[e]	56	56.0	174.8	3.1	1.76	1.45	1.57	1.42	Transparent, rigid

[a] Molar percentage of the BSPA containing component.
[b] Calculated from the copolymer composition.
[c] Determined by titration.
[d] Obtained from the ^{1}H NMR spectrum.
[e] After thermal treatment at 150 °C.
[f] Not measured.

calculated from the integral ratio in the ^{1}H NMR spectra. For example, the IEC value of SPI-8(50)-*m* was determined from the integral ratio of the peaks, *f*: (*j* + *k* + *l*) in Figure 1. The obtained IEC values were in fair agreement with the ones expected from the feed monomer ratios. The experimentally obtained IEC of SPI-14H was slightly lower than that of SPI-14, supporting the above claim that a small amount of cross-linking was contained in the SPI-14H via thermal dehydration reactions of acid groups. Casting DMSO solutions of SPI-8-*m*, -8-*p*, -9, -10, and -14H gave membranes with the thickness of ~50 μm. The obtained membranes were of brown color typical for polyimides with toughness and flexibility. SPI-11, -12, and -13 gave rather brittle membranes due to their insufficient molecular weight, which made them unavailable for the properties analyses. Similar to SPI-8-*p*,[16] SPI-8-*m* and -10 containing 1H-1,2,4-triazole groups gave somewhat turbid membranes, whereas the SPI-9 and -14H membranes were transparent. The linear and rod-like structure of triazole groups in the polymer backbone would be responsible for possibly higher crystallinity of SPI-8-*p*, SPI-8-*m*, and -10 membranes. The IEC values obtained by titration were slightly lower than the ones obtained from the feed monomer ratios and ^{1}H NMR spectra. The results may suggest that a small portion of sulfonic acid groups interact with NH and COOH groups.

Thermal, Oxidative, and Hydrolytic Stability

The thermal stability of SPI copolymers (SPI-8-*m*, -9, -10, and -14H) was investigated by TG/DTA-MS analyses under dry Ar atmosphere (Fig. 2). In the TGA curves, two-step weight losses were observed from room temperature to 180 °C and above 200 °C. By combining TG with MS chromatograms, the first gradual weight loss was assigned to the evaporation of hydrated water (H_2O = 18 *m/z*) and the second more rapid weight loss was due to the decomposition of SPIs. The major fragment ions observed in the second weight loss were SO = 48 and SO_2 = 64 *m/z*, indicating that the thermal decomposition commenced by the loss of sulfonic acid groups in the side chains. The TG curves of SPI-8-*m*, -9, -10, and -14H were similar to that of SPI-8-*p*,[16] because they share the same hydrophilic component (BSPA). In the DTA curves of SPIs, no glass transition temperatures were observed below the decomposition temperatures.

Oxidative and hydrolytic stability of the SPI membranes were tested under accelerated testing conditions. In both experiments, changes in weight, IEC, and molecular weight of the membranes were plotted as a function of IEC in Figures 3 and 4. For comparison, the stability data are also given for NRE212 membrane; NRE212 membrane was intact even under the harsh conditions. The oxidative stability of SPI membranes were evaluated in hot Fenton's reagent for 1 h. The SPI membranes showed relativity good stability to oxidation with only minor weight losses. Although SPI-14H membrane showed large decrease in IEC, the other membranes lost less than 12% of the pristine IEC values. All SPI membranes investigated showed large loss in molecular weight. Among them, SPI-10 was the most stable. The results indicate that the oxidative degradation involves main chain scission and 1H-1,2,4-triazole groups directly attached to imide linkages at 3,5-positions contributed to improving the oxidative degradation.

The hydrolytic stability of SPI membranes was evaluated in pressurized water at 140 °C for 24 h. The SPI-8-*m*, -8-*p*, -9, and -14H membranes showed high hydrolytic stability with small changes in weight and IEC value. Unlike the above oxidative stability, SPI-10 membrane showed larger loss in molecular weight. This is probably because SPI-10 membrane with the higher IEC (1.95 mequiv g^{-1}) and lower molecular weight than other ionomers dissolved into water (100% weight loss) and was hydrolyzed faster in aqueous solution. In these accelerated stability testings, major degradation mechanism was the main chain scission via hydrolysis of imide bonds. NH- and COOH-containing groups in the polymer backbone seemed to have minor effect on the stability of SPI membranes under wet conditions.

Mechanical Properties

Mechanical properties of the SPI membranes were evaluated with tensile testing at 85 °C and 93% RH and are shown in

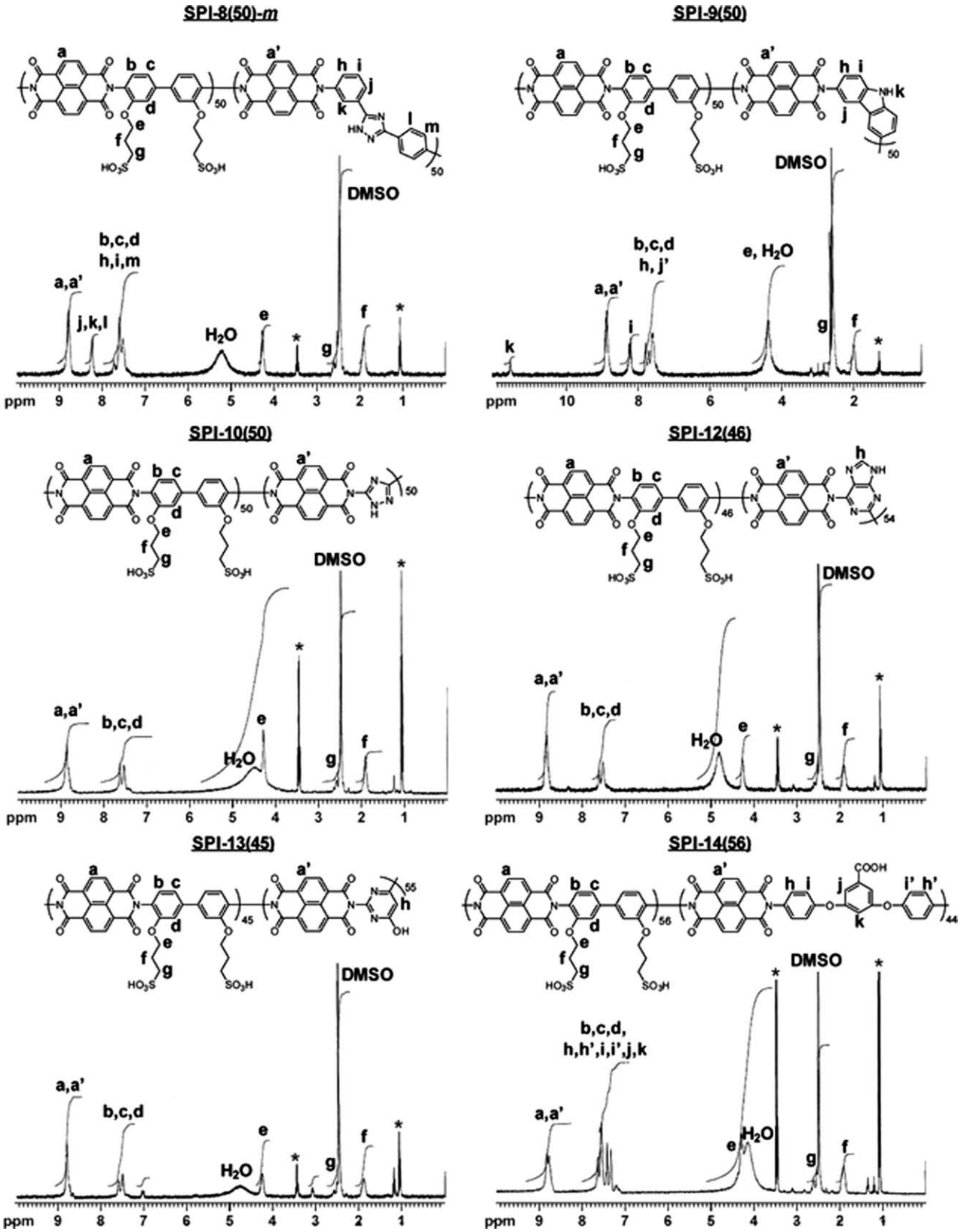

FIGURE 1 ^{1}H NMR spectra of SPI-8-*m*, -9, -10, -12, -13, and -14 in DMSO-d_6. *Peaks derived from residual solvent (ethanol).

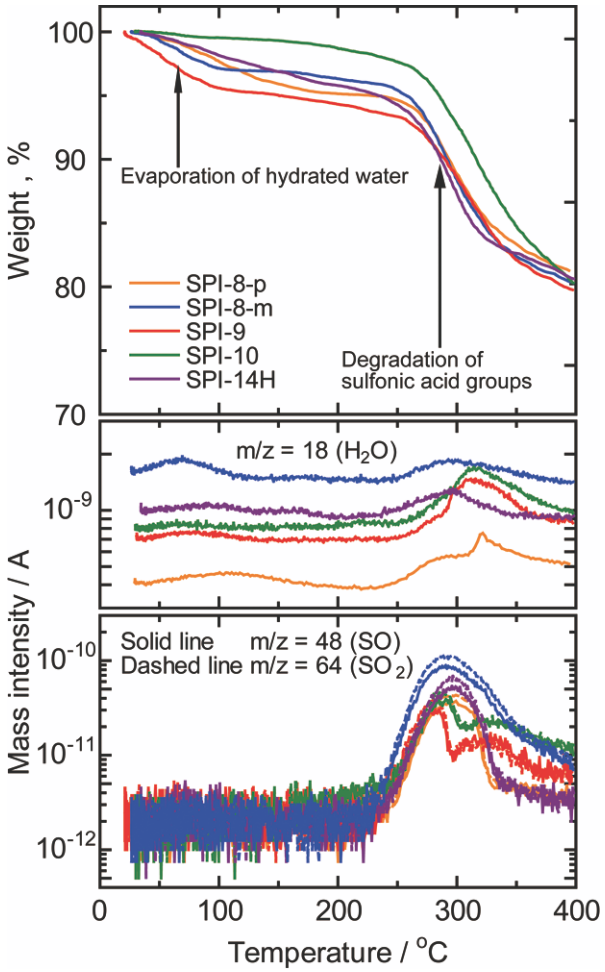

FIGURE 2 TG/DTA and MS curves of SPI membranes under Ar atmosphere.

Figure 5. SPI membranes exhibited better mechanical properties, higher maximum stress (>22 MPa) and lower elongation at break (<52%) than those of NRE212 membrane. The SPI-8-*p* membrane showed the highest maximum stress. The SPI-8-*m* and SPI-10 membranes showed the highest Young's modulus (1.5 GPa), whereas that of SPI-9 and -14H membranes was rather low (0.95 and 0.61 GPa, respectively; Table 2). These two membranes were transparent and probably less crystalline than SPI-8-*m*, -8-*p*, and -10 membranes.

Then, we carried out the DFT calculation of the NH- and COOH-containing units to estimate roughly their structure

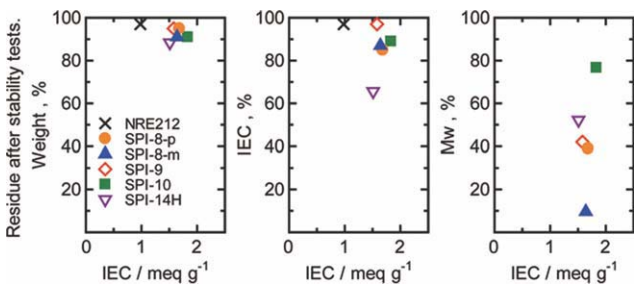

FIGURE 3 Oxidative stability of SPI and NRE212 membranes.

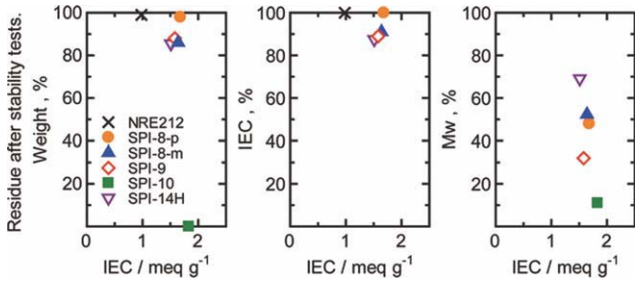

FIGURE 4 Hydrolytic stability of SPI and NRE212 membranes.

and interaction with acid groups. The calculation results revealed that the NH-containing units in SPI-8-*p*, -8-*m*, -9, and -10 have compact structures and COOH-containing unit of SPI-14 is distorted and bulky due to the flexible ether bonds (see Supporting Information Fig. S3). The binding energy of these components with methanesulfonic acid, supposing that the atoms having the highest elctoro-negativity interact with sulfonic acid groups, is in the order of SPI-14H > SPI-10 > SPI-8-*m* > SPI-8-*p* > SPI-9 (see Supporting Information Table S1). Except for SPI-14H, the order is in good agreement with the results of Young's moduli. As carboxylic acid group can interact strongly with sulfonic acid group by participating two points hydrogen bondings, the binding energy of the model component of SPI-14H was higher than that of the others. However, in the bulk polymer membrane, this would not be the case due to the tortuosity of the structure of SPI-14.

On the other hand, density of the membranes was not in the same order (Table 1); SPI-8-*m* (1.75 g cm^{-3}) > SPI-9 (1.60 g cm^{-3}) > SPI-8-*p* (1.49 g cm^{-3}) > SPI-10 (1.47 g cm^{-3}) > SPI-14H (1.42 g cm^{-3}). The results may indicate that, in some cases such as SPI-9, intermolecular interactions (either π–π and/or NH-acid interaction) are relatively weak even when the polymer chains are densely packed.

Gas Permeability

Temperature dependence of dry hydrogen and oxygen permeability coefficient (Q) of SPI-8-*p*, -8-*m*, -14H, and NRE212 membranes is shown in Figure 6. Results of SPI-9 and -10 could not be obtained because the membranes were not strong enough and broke during the measurements. The SPI-8-*p*, -8-*m*, and -14H membranes showed lower gas permeability for both hydrogen and oxygen than that of NRE212. SPI membranes showed lower activation energy of the gas permeability than that of NRE212 as is obvious from the slope in the Arrhenius plots [E_a (H_2) = 39 and E_a (O_2) = 53 kJ mol^{-1} (NRE212), E_a (H_2) = 17 and E_a (O_2) = 14 kJ mol^{-1} (SPI-8-*p*), E_a (H_2) = 18 and E_a (O_2) = 19 kJ mol^{-1} (SPI-8-*m*), E_a (H_2) = 18 and E_a (O_2) = 15 kJ mol^{-1} (SPI-14H), respectively]. The lower gas permeability of SPI membranes was more pronounced at higher temperature. Compared with SPI-8-*p* and SPI-14H membranes, SPI-8-*m* membrane showed slightly lower gas permeability. The results are reasonably explained by the density data. SPI-8-*m* membrane has higher density (1.75 g cm^{-3}) than that of SPI-8-*p* (1.49 g cm^{-3}) and SPI-14H (1.42 g cm^{-3}) membranes. As gases

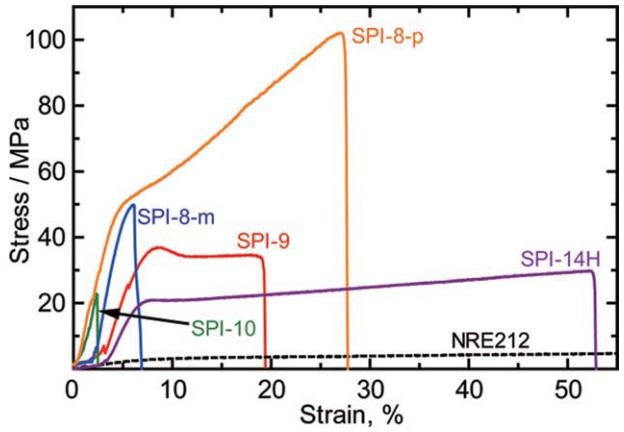

FIGURE 5 Stress versus strain curves of SPI and NRE212 membranes at 85 °C and 93% RH. [Color figure can be viewed in the online issue, which is available at www.interscience.wiley.com.]

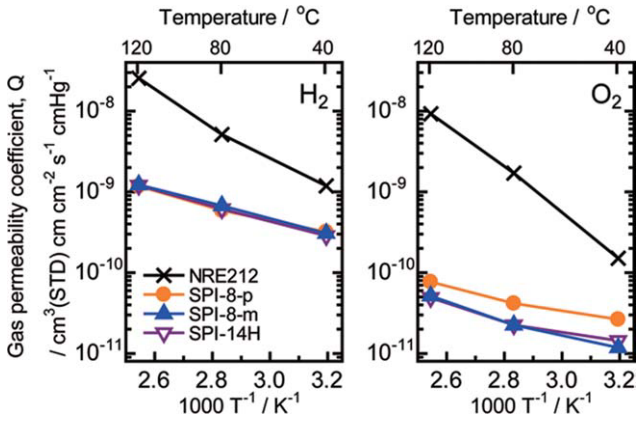

FIGURE 6 Temperature dependence of dry hydrogen and oxygen permeability of SPI-8-*p*, -8-*m*, -14H, and NRE212 membranes. [Color figure can be viewed in the online issue, which is available at www.interscience.wiley.com.]

would mainly permeate through free volume in membranes, it is considered that the SPI-8-*m* membrane with higher density showed the lowest gas permeability. SPI-14H membrane showed lower gas permeability, especially oxygen, than that of SPI-8-*p*. Possible explanation would be that heterocyclic triazole moieties have affinity to oxygen and could solubilize more oxygen molecules.

Water Uptake and Proton Conductivity

Humidity dependence of water uptake and proton conductivity were measured at 80 °C for SPI membranes (Fig. 7). The measurement was carried out by repeating sorption and desorption processes and the data in Figure 7 were obtained during the sorption process. The SPI-8-*m*, -9, and -10 membranes showed slightly lower water uptake than that of SPI-8-*p* membrane at all humidities, and the water uptake of SPI-14H membrane was higher than that of SPI-8-*p* (except at high humidity). The high water absorbability of SPI-14H, despite of its low IEC and partly crosslinked structure, is presumably due to weaker intermolecular interaction as suggested by the mechanical properties, DFT calculation, and density measurement.

The proton conductivity of SPI membranes was not in the same order as their water uptake. The SPI-8-*p* membrane showed the highest proton conductivity at high humidity (>60% RH). SPI-14H membrane showing high water uptake also showed high proton conductivity. In contrast, the SPI-8-*m* and -9 membranes exhibited higher proton conductivity at low humidity than that of SPI-8-*p* in spite of the formers' lower water absorbability.

TABLE 2 Mechanical Properties of SPI Membranes at 85 °C and 93% RH

Membrane	Maximum Stress (MPa)	Elongation at Break (%)	Young's Modulus (GPa)
SPI-8-*p*	103	28	1.2
SPI-8-*m*	50	7	1.5
SPI-9	37	19	0.95
SPI-10	22	3	1.5
SPI-14H	29	52	0.61

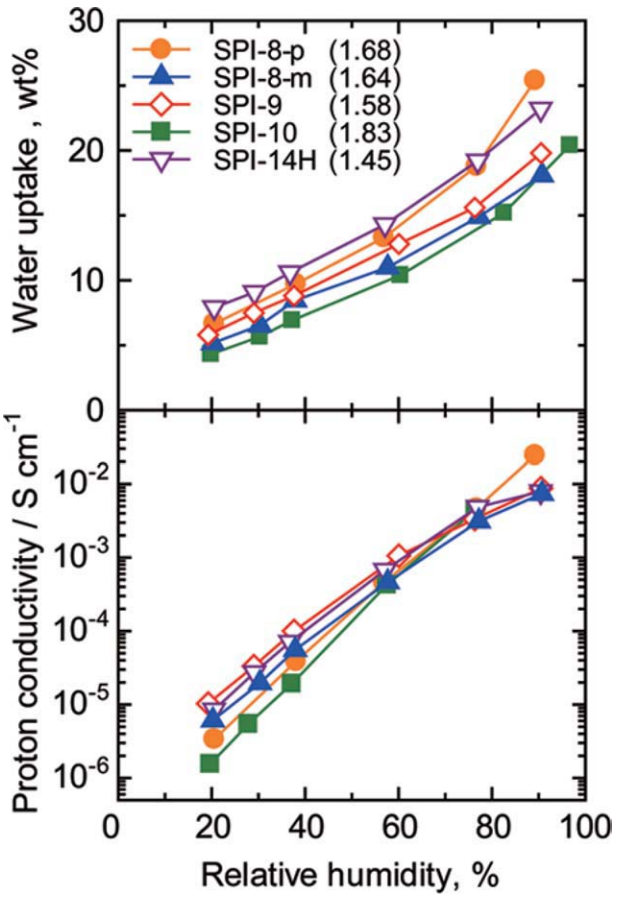

FIGURE 7 Humidity dependence of the water uptake and proton conductivity of SPI membranes (IEC, mequiv g^{-1} in parentheses) at 80 °C. [Color figure can be viewed in the online issue, which is available at www.interscience.wiley.com.]

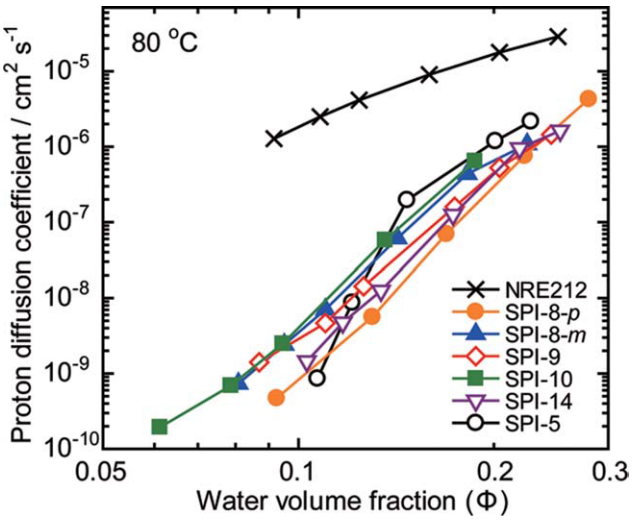

FIGURE 8 Proton diffusion coefficient of SPI membranes as a function of water volume fraction at 80 °C. [Color figure can be viewed in the online issue, which is available at www.interscience.wiley.com.]

For more detailed investigation, the proton conductivity was plotted as a function of number of absorbed water molecules per sulfonic acid (λ), which takes into account both water uptake and IEC, for SPIs and compared with that of our previous SPI (SPI-5)[19] containing aliphatic segments in place of NH- or COOH-containing groups (see Supporting Information Fig. S4). Except for SPI-14H membrane, the new SPI membranes showed higher proton conductivity at low λ value ($\lambda < 5$) than that of SPI-5. The most pronounced effect was observed in SPI-10, which contains 1H-1,2,4-triazole groups directly attached to imide linkages at 3,5-positions.

The proton diffusion coefficient (D_σ) of SPI membranes was calculated with the Nernst-Einstein equation regarding water volume and concentration of proton charge carrier in polymer electrolyte membranes. D_σ value of SPI membranes was plotted in Figure 8 as a function of water volume fraction (Φ) at 80 °C. The proton diffusivity of NRE212 was much higher than those of the SPI membranes, and the difference between NRE212 and SPIs became larger at lower Φ. The results suggest that NRE212 membrane utilizes water more efficiently for the proton conduction at low water content. At lower Φ, D_σ of the current SPI membranes was higher than that of SPI-5. Among the SPIs, SPI-8-*m*, -9, and -10 membranes showed relativity higher D_σ values at lower Φ. The NH groups, either within triazole or carbazole rings, were most effective in improving the proton transport properties in the SPI membranes.

EXPERIMENTAL

Materials

1,4,5,8-Naphthalenetetracarboxylic dianhydride (TCND) (>97%, Lancaster), 3,6-diaminocarbazole (>98%, TCI), 3,5-diamino-1H-1,2,4-triazole (>97%, TCI), bis(3-aminopropyl)-amine (>98%, TCI), 2,6-diaminopurine (>97%, TCI), 2,4-diamino-6-hydroxyprymidine (>98%, TCI), and 3,5-bis(4-aminophenoxy)benzoic acid (>95%, TCI) were used as received. 3,3′-Bis(sulfopropoxy)-4,4′-diaminobiphenyl (BSPA) was synthesized from 3,3′-dihydroxy benzidine (98%, TCI) and 1,3-propanesultone (Kanto Chemical) according to the literature.[20] 3,5-Bis(4-aminophenyl)-1H-1,2,4-triazole (*p*-APTAZ) was synthesized according to the literature.[16] These monomers were characterized by ^{1}H NMR spectroscopy and stored in the dark. TEA (Aldrich) and benzoic acid (Kanto Chemical) were used as received. *m*-Cresol (Kanto Chemical) was dried over molecular sieves 3 Å before use. Other chemicals were of commercially available grade and used as received.

3-(4-Aminophenyl)-5-(3-aminophenyl)-1H-1,2,4-triazole (*m*-APTAZ)

m-APTAZ was synthesized from 4-aminobenzohydrazide (98%, TCI) and 3-aminobenzonitrile (98%, TCI) according to the literature.[21] This monomer was characterized by liquid chromatography/mass spectroscopy (LC/MS) and ^{1}H NMR spectroscopy, and stored in the dark.

Polymerization

A typical procedure for the copolymerization is as follows. BSPA (1.0 mmol), 3,6-diaminocarbazole (1.0 mmol), TEA (10.8 mmol), and 10 mL of *m*-cresol were placed in a four-neck round-bottomed flask equipped with a magnetic stirring bar and N_2 inlet. The mixture was stirred at 100 °C until dissolved. After clear solution was obtained, the mixture was cooled to room temperature and stirred under a stream of N_2. TCND (2.0 mmol) and benzoic acid (4.0 mmol) were then added into the mixture. The mixture was heated at 175 °C for 15 h and at 195 °C for 3 h. After the reaction, the mixture was poured dropwise into a large excess of acetone. A yellow powder of the precipitate was filtered, washed with acetone, and dried at 80 °C under reduced pressure for 12 h to obtain SPI-9(50) as triethylammonium form. The other copolymers, SPI-8-*m*(50), -8-*p*(50), -10(50), -11(46), -12(46), -13(45), and -14(56), were synthesized in a similar manner.

Membrane Preparation

The copolymers (0.4 g) were dissolved in 10 mL of dimethyl sulfoxide (DMSO) and cast onto a flat glass plate. After drying at 55 °C, crude membrane in triethylammonium form was immersed in ethanol containing 1 N HNO_3 for 30 min at 50 °C. The acidification procedure was repeated three times followed by washing with pure ethanol. After drying at 80 °C under reduced pressure for 12 h, the copolymer membranes in acid form (~50 μm thick) were obtained.

Measurements

^{1}H (400 MHz) NMR spectra were recorded on a Bruker AVANCE 400S spectrometer with deuterated dimethyl sulfoxide (DMSO-d_6) or deuterated water (D_2O) as a solvent and tetramethylsilane (TMS) as an internal reference. LC/MS experiments were performed on a Shimadzu SPD-M10Avp (column: Shodex VP-ODS) and a Shimadzu LCMS-2010A. Molecular weight was measured with gel permeation chromatography

(GPC) equipped with two Shodex KF-805 columns and a Jasco 805 UV detector set at 300 nm with DMF containing 0.01 M LiBr as eluent. Molecular weight was calibrated with standard polystyrene samples. IEC of the SPI membranes was determined by ^{1}H NMR spectra and titration. In the titration method, a piece of membrane samples was equilibrated in large excess of 0.1 M NaCl aq solution at 40 °C for one day. The amount of HCl released from the membrane samples was measured by titration with 0.01 N NaOH aq solution. Density of dry SPI membranes was measured by pycnometer (Ultrapycnometer1000, Quantachrome Inc.) using helium as test gas at room temperature. Density at 80 °C was calibrated using the volume expansion coefficient of perfluoroalkyl polymer (PFA: 1.3×10^{-4} K^{-1}) and polyimide (PI: 4.0×10^{-5} K^{-1}), as the coefficient of NRE212 and SPIs were not available.

Thermal Properties

Thermal analyses were performed via TG/DTA-MS with a Mac Science TG/DTA 2000 equipped with a Bruker MS 9600 mass spectrometer at a heating rate of 5 °C min^{-1} under argon.

Oxidative Stability

A small piece of membrane sample was soaked in Fenton's reagent (3% H_2O_2 containing 2 ppm $FeSO_4$) at 80 °C for 1 h. The stability was evaluated by changes in IEC, weight, and molecular weight of the test samples.

Hydrolytic Stability

A small piece of membrane sample was treated in water at 140 °C for 24 h. The stability was evaluated by changes in IEC, weight, and molecular weight of the test samples.

Mechanical Strength

Tensile testing was performed with a Shimadzu universal testing instrument Autograph AGS-J500N equipped with a chamber, in which temperature and humidity were controlled by flowing humidified air with a Toshin Kogyo temperature control unit Bethel-3A. Stress versus strain curves were obtained at a stretching rate of 10 mm min^{-1} for samples cut into a dumbbell shape [DIN-53,504-S3, 35 mm × 6 mm (total) and 12 mm × 2 mm (test area)].

Gas Permeability

Hydrogen and oxygen permeability through the ionomer membrane was measured with a GTR-Tech 20XFYC gas permeation measurement apparatus equipped with a Yanaco G2700T gas chromatography. The gas chromatography contained a Porapak-Q column and a TCD detector. Argon and helium were used as a carrier gas for the measurement of hydrogen and oxygen, respectively. A membrane sample (φ = 30 mm) was set in a cell that has a gas inlet and outlet on both sides of the membrane. Placing it in an oven controlled the cell temperature. On one side of the membrane, dry test gas (hydrogen or oxygen) was supplied at a flow rate of 30 mL min^{-1}, whereas on the other side of the membrane, the same gas as the carrier used in the gas chromatograph (flow gas) was supplied at a flow rate of 30 mL min^{-1}. Before each measurement was done, the membrane was equilibrated with the gases at the given temperature for at least 3 h. Then, 3.7 mL of flow gas was sampled and subjected to the gas chromatography to quantify the test gas permeated through the membrane. The gas permeability coefficient, Q (cm^3 (STD) cm cm^{-2} s^{-1} cmHg^{-1}), was calculated according to the following equation:

$$Q = \frac{273}{T}\frac{1}{A}B\frac{1}{t}l\frac{1}{76}$$

where T (K) is the absolute temperature of the cell, A (cm^2) is the permeation area, B (cm^3) is the volume of test gas permeated through the membrane, t (s) is the sampling time, and l (cm) is the thickness of the membrane.

Water Uptake and Proton Conductivity

Water uptake and proton conductivity of the SPI membranes were measured with a Bel Japan solid electrolyte analyzer system MSB-AD-V-FC equipped with a chamber, a magnetic suspension balance, and a four-point probe conductivity cell. For water uptake measurement, membrane samples (40–60 mg) were set in a chamber and dried at 80 °C under vacuum for 3 h until constant weight as dry materials was obtained. The membrane was equilibrated with N_2 gas at given temperature and humidity for at least 1 h before the gravimetry was done. For the proton conductivity measurement, membrane samples (1.0 cm wide and 3.0 cm long) were set in the chamber where the temperature and the humidity were controlled by flowing humidified N_2. The membrane was equilibrated with N_2 gas at the set temperature and humidity for at least 1 h before the measurement. The samples were contacted with two gold wire outer current-carrying electrodes and two gold wire inner potential-detecting electrodes. Impedance measurements were carried out with a Solartron 1255B frequency response analyzer and a Solartron SI 1287 potentiostat. The instrument was used in potentiostatic mode with an ac amplitude of 300 mV with the frequency range from 10 to 100,000 Hz.

From the proton conductivity and density data, the proton diffusion coefficient (D_σ) was calculated according to the following equations:

$$D_\sigma = \frac{RT}{F^2}\frac{\sigma}{c(H^+)}$$

where R is the gas constant, T is the absolute temperature (K), F is Faraday constant, and $c(H^+)$ is the concentration of the proton charge carrier (mol L^{-1}).

Computational Calculation

The computational calculations were carried out for optimized geometries, atomic charges, and ground-state energy with Gaussian 03W program. All calculations were performed at the Density Functional Theory (DFT) method with the B3LYP (B3:Becke's three-parameter, LYP: Lee-Yang-Parr) functional and with a reasonably large basis set of 6-31G(d,p).

CONCLUSIONS

We have synthesized a new polyimide ionomers (SPI-8 – 14) containing NH, OH, or COOH groups in the polymer

backbone. Among them, SPI-8-*m*, -8-*p*, -9, -10, and -14H containing triazole, carbazole, and carboxylic acid groups gave tough and flexible membranes by solution casting. These SPI membranes were thermally stable up to 200 °C without glass transition and decomposition. Oxidative and hydrolytic stability was confirmed by accelerated testings. All SPI membranes showed relativity good oxidative stability, whereas the effect of the NH and COOH-containing groups seemed limited since the major degradation mechanism was scission of the imide linkages. SPI-8-*p*, -8-*m*, and -10 membranes containing triazole groups exhibited high mechanical strength due to their possibly high crystallinity. Hydrogen and oxygen permeability of SPI-8-*p*, -8-*m*, and -14H membranes was much lower than that of NRE212 at wide range of temperature. Triazole and carbazole groups had an impact on the proton conducting properties of SPI membranes at low humidity (or low water content). However, the conductivity was still lower than that of NRE212 and therefore, further molecular consideration such as block copolymer architecture would be needed.

This work was partly supported by the New Energy and Industrial Technology Development Organization (NEDO) through HiPer-FC Project, and the Ministry of Education, Culture, Sports, Science and Technology (MEXT), Japan, through a Grant-in-Aid for Scientific Research. The authors thank K. Yagi of University of Yamanashi for his help with computational calculation.

REFERENCES AND NOTES

1 Kordesch, K.; Simader, G. Fuel Cells and Thier Applications; VCH: Weinheim, Germany, 1996.

2 Appleby, A. J.; Foulkes, F. R. Fuel Cell Handbook; Van Nostrand Reinhold: New York, 1989.

3 Carrette, L.; Friedrich, K. A.; Stimming, U. Fuel Cells 2001, 1, 5–39.

4 Steele, B. C. H.; Heinzel, A. Nature 2001, 414, 345–352.

5 Miyatake, K.; Watanabe, M. Electrochemistry 2005, 73, 12–19.

6 Vallejo, E.; Pourcelly, G.; Gavach, C.; Mercier, R.; Pineri, M. J Membr Sci 1999, 160, 127–137.

7 Genies, C.; Mercier, R.; Sillion, B.; Cornet, N.; Gebel, G.; Pineri, M. Polymer 2001, 42, 359–373.

8 Fang, J.; Guo, X.; Harada, S.; Watari, T.; Tanaka, K.; Kita, H.; Okamoto, K.–I. Macromolecules 2002, 35, 9022–9028.

9 Guo, X.; Fang, J.; Watari, T.; Tanaka, K.; Kita, H.; Okamoto, K.-I. Macromolecules 2002, 35, 6707–6713.

10 Miyatake, K.; Zhou, H.; Watanabe, M. Macromolecules 2004, 37, 4956–4960.

11 Matsumoto, K.; Nakagawa, T.; Higashihara, T.; Ueda, M. J Polym Sci A: Polym Chem 2009, 47, 5827–5834.

12 Roy, A.; Hickner, M. A.; Einsla, B. R.; Harrison, W. L.; McGrath, J. E. J Polym Sci A: Polym Chem 2009, 47, 384–391.

13 Miyatake, K.; Yasuda, T.; Watanabe, M. J Polym Sci A: Polym Chem 2008, 46, 4469–4478.

14 Sutou, Y.; Yin, Y.; Hu, Z.; Chen, S.; Kita, H.; Okamoto, K.-I.; Wang, H.; Kawasato, H. J Polym Sci A: Polym Chem 2009, 47, 1463–1477.

15 Borup, R.; Meyers, J.; Pivovar, B.; Kim, Y. S.; Mukundan, R.; Garland, N.; Myers, D.; Wilson, M.; Garzon, F.; Wood, D.; Zelenay, P.; More, K.; Stroh, K.; Zawodzinski, T.; Boncella, J.; McGrath, J. E.; Inaba, M.; Miyatake, K.; Hori, M.; Ota, K.; Ogumi, Z.; Miyata, S.; Nishikata, A.; Siroma, Z.; Uchimoto, Y.; Yasuda, K.; Kimijima, K.-I.; Iwashita, N. Chem Rev 2007, 107, 3904–3951.

16 Saito, J.; Miyatake, K.; Watanabe, M. Macromolecules 2008, 41, 2415–2420.

17 Kabasawa, A.; Saito, J.; Yano, H.; Miyatake, K.; Uchida, H.; Watanabe, M. Electrochim Acta 2009, 54, 1076–1082.

18 Kabasawa, A.; Saito, J.; Miyatake, K.; Uchida, H.; Watanabe, M. Electrochim Acta 2009, 54, 2754–2760.

19 Asano, N.; Aoki, M.; Suzuki, S.; Miyatake, K.; Uchida, H.; Watanabe, M. J Am Chem Soc 2006, 128, 1762–1769.

20 Zhou, H.; Miyatake, K.; Watanabe, M. Fuel Cells 2005, 5, 296–301.

21 Yeung, K.-S.; Farkas, M. E.; Kadow, J. F.; Meanwell, N. A. Tetrahedron Lett 2005, 46, 3429–3432.